

Mind-to-Face: Neural-Driven Photorealistic Avatar Synthesis via EEG Decoding

Haolin Xiong^{1,2*}, Tianwen Fu^{1,2*}, Pratusha Bhuvana Prasad^{1,2}, Yunxuan Cai^{1,2},
Haiwei Chen^{1,2}, Wenbin Teng^{1,2}, Hanyuan Xiao^{1,2}, Yajie Zhao^{1,2†}

¹Institute for Creative Technologies

²University of Southern California

{hx_624, tianwenf}@usc.edu, bprasad@ict.usc.edu, yunxuanc@usc.edu,
chenh@ict.usc.edu, {wenbinte, hanyuanx}@usc.edu, zhao@ict.usc.edu

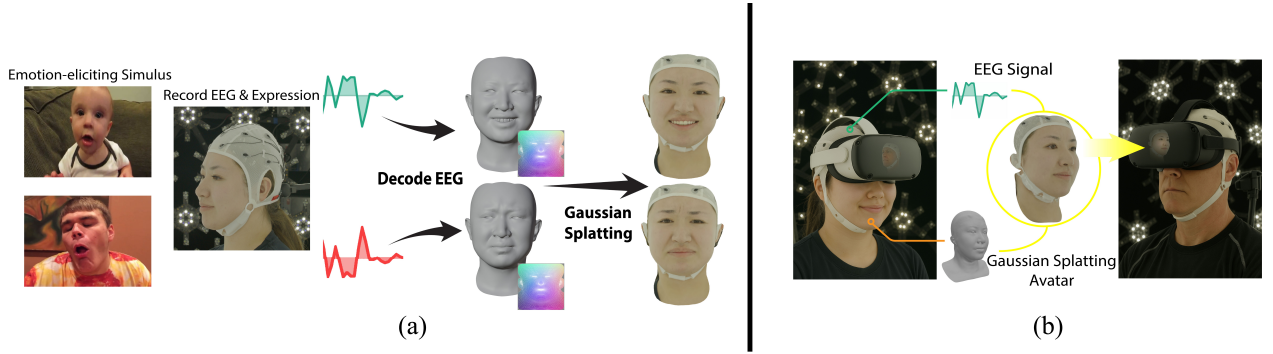


Figure 1. Overview of Mind-to-Face, our neural-driven avatar framework. (a) We record synchronized EEG and facial expressions while subjects view emotion-eliciting stimuli, then decode the EEG into dense 3D position maps, and render photorealistic avatars using 3D Gaussian Splatting [14]. (b) Although AR/VR is not the primary focus of this work, a potential use case is shown: EEG can be decoded to drive an expressive avatar even when the face is fully occluded by a head-mounted display.

Abstract

Current expressive avatar systems rely heavily on visual cues, failing when faces are occluded or when emotions remain internal. We present **Mind-to-Face**, the first framework that decodes non-invasive electroencephalogram (EEG) signals directly into high-fidelity facial expressions. We build a dual-modality recording setup to obtain synchronized EEG and multi-view facial video during emotion-eliciting stimuli, enabling precise supervision for neural-to-visual learning. Our model uses a CNN-Transformer encoder to map EEG signals into dense 3D position maps, capable of sampling over 65k vertices, capturing fine-scale geometry and subtle emotional dynamics, and renders them through a modified 3D Gaussian Splatting pipeline for photorealistic, view-consistent results. Through extensive evaluation, we show that EEG alone can reliably predict dynamic, subject-specific facial expressions, including subtle emotional responses, demonstrating that neural signals contain far richer affective and geometric information than previously assumed. **Mind-to-Face** establishes a new paradigm for

neural-driven avatars, enabling personalized, emotion-aware telepresence and cognitive interaction in immersive environments.

1. INTRODUCTION

Current expressive avatar systems rely heavily on visual cues, yet full-face imagery is often unavailable due to Head-mounted Display’s (HMD) occlusion, privacy constraints, or muscular impairments. In contrast, biosignals such as EEG can be captured unobtrusively with consumer-grade hardware, yet existing cognitive science research typically maps them only to coarse, discrete emotion labels, leaving their potential for reconstructing continuous, full-facial expressions largely unexplored.

We present Mind-to-Face, a framework that bridges neural activity and high-fidelity facial expression, enabling communication that reflects what the brain experiences rather than what cameras capture. Our approach addresses three core challenges. First, we design a dual-modality data acquisition setup that synchronously records Electroencephalography (EEG) signals and multi-view facial video during emotion-eliciting stimuli, solving a key engi-

*Equal Contribution

†Corresponding author.

neering challenge in aligning neural activity with visual expression. Second, we introduce a neural decoding pipeline that translates EEG patterns into photorealistic renderings via 3D Gaussian Splatting. Because neural responses are highly individualized, *i.e.* identical stimuli can produce distinct EEG signatures across subjects, we focus on personalized neural-to-expression mappings as the basis for subject-specific digital doubles, prioritizing expressive accuracy over population-level generalization.

EEG is a non-invasive method for measuring electrical brain activity and is widely used in brain-computer interfaces (BCIs). Prior work demonstrates strong correlations between EEG signals and emotional states [5, 55] or symbolic facial expressions [54], indicating their potential for decoding expressive information directly from brain activity. However, despite increasing interest in EEG-based applications, EEG has rarely been used as a driver for visual synthesis. Recent learning-based approaches classify discrete expression labels from EEG [19, 21], but remain limited to coarse categories and cannot capture the continuous, fine-grained dynamics required for realistic avatar control. Achieving high-fidelity reconstruction from EEG is challenging due to the low dimensionality and noisiness of neural signals.

To overcome this challenge and improve expressive fidelity, we adopt a CNN-Transformer hybrid encoder inspired by EEG-Conformer [40], capturing both local spatial correlations and long-range temporal dependencies in EEG. Each EEG slice is encoded into a latent representation of brain activity, which is then decoded into a dense 3D position map [23] to produce continuous facial geometry in UV space. Unlike strain-gauge systems [17], EEG offers a richer and more holistic measure of cognitive and affective states. For photorealistic rendering, we build on the 3D Gaussian Splatting framework [14] following GaussianAvatars [31], but replace the low-dimensional FLAME model [20] with a high-degree-of-freedom 3D position map. This dense representation captures subtle geometric details and fine expression nuances that are smoothed out in low-dimensional models. We further modify the deformation and skinning system of GaussianAvatars to support this representation and incorporate a robust facial-tracking pipeline during preprocessing, enabling accurate reconstruction even under occlusion and challenging expressions.

In summary, our key contributions include:

1. We introduce *Mind-to-Face*, the first system that decodes non-invasive EEG signals into dense 3D facial geometry and renders photorealistic avatars. Our approach establishes a continuous neural-to-visual mapping, enabling expressive facial motion to be reconstructed directly from brain activity.
2. We design a custom **dual-modality data acquisition**

system that synchronously records 16-channel EEG signals and high-speed multi-view facial videos while subjects watch emotion-eliciting film clips. This setup provides precise temporal alignment between neural activity and visible facial responses, producing the first dataset that supports supervised learning for neural-driven 3D facial synthesis and enabling new research directions in neural decoding, telepresence, and affective computing.

3. We propose a **dense 3D position-map representation** as an alternative to low-dimensional FLAME/blendshape controls, and integrate it with a modified 3D Gaussian Splatting (3DGS) renderer. This representation captures fine-scale geometry and subtle expression cues, enabling lifelike, emotionally consistent avatars that reflect individualized neural responses.

2. RELATED WORK

2.1. EEG Decoding and Emotion Recognition

Electroencephalography (EEG) decoding is an active area of research in brain-computer interface (BCI), emotion recognition, and cognitive state estimation [42]. Traditional approaches rely on handcrafted features such as band power [52], Common Spatial Patterns (CSP) [28], or functional connectivity [49] to summarize EEG into low-dimensional descriptors, often limiting the richness of information available for learning expressive behaviors. Recent advances leverage deep learning to directly extract spatial and temporal features from raw EEG. Convolutional networks (CNNs) are widely used for spatial filtering across channels [16, 32, 40], while RNNs [29] and Transformers [39, 40] have been explored for temporal modeling.

There are two primary theoretical models for representing human emotions. The first is the discrete model, which categorizes emotions into a fixed set of basic classes—originally six, as introduced by Ekman [6], and later expanded to include up to fifteen [27]. In contrast, the dimensional model represents emotions along continuous axes such as arousal, valence, pleasure, displeasure, sleepiness, and distress, as proposed by Russell [34]. These models have been widely adopted in emotion recognition research and dataset design.

Early EEG-based emotion recognition systems [24, 37] visualized categorical emotional states using digital avatars. The SEED dataset [53] introduced a collection of EEG recordings for tasks including sleep state detection, eye blink detection, and emotion classification. The publicly available dataset most similar to our setting is MAHNOB-HCI [36], which includes one RGB and five monochrome facial video streams synchronized with 32-channel EEG recordings. However, due to its low resolution and monochrome format, MAHNOB-HCI cannot be used for

3D facial reconstruction. To the best of our knowledge, our Mind-to-Face data capture setting is the first to collect a high-fidelity multi-view dataset that enables photogrammetric 3D face reconstruction synchronized with EEG signals as well as stimuli videos.

2.2. Head Reconstruction and Neural Avatars

Recent advances in differentiable rendering and implicit scene representations have substantially improved the realism and controllability of digital head avatars. Thies et al. [45] introduced a real-time face tracking and transfer system, establishing the foundation for neural avatar animation. Subsequent progress in face image synthesis [3, 46] has enabled more expressive control over facial expressions, lip synchronization, and head motion [15, 43, 50].

More recently, Neural Radiance Field (NeRF)-like methods [25] have since emerged as a powerful paradigm for realistic head avatar modeling and rendering. Gafni et al. [8] learn a dynamic NeRF conditioned on expression vectors from monocular video input, while Grassal et al. [9] extend the FLAME model [20] by subdividing the mesh and introducing expression-dependent geometric and texture offsets to enhance realism. Other approaches, such as IMavatar [56], employ neural implicit functions to model avatars and solve for deformations between observed and canonical poses via iterative root-finding.

Since 2023, 3D Gaussian Splatting (3DGS) [14] has emerged as a powerful yet efficient alternative to NeRF-like methods. A growing body of work has explored 3DGS for human avatar animation, including controllable full-body avatars [10, 57], motion synthesis [26, 51], and head reconstruction [44]. Notably, GaussianAvatars [31] introduced a framework that combines FLAME-based explicit expression control with 3DGS rendering, achieving high-fidelity geometry and photorealistic appearance through anisotropic splatting. Importantly, while preserving the fine-grained visual fidelity of NeRFs, 3DGS offers an explicit scene representation that enables precise control over geometry and appearance, making it particularly well-suited for animation tasks.

Our work builds upon the rendering paradigm of GaussianAvatars [31]. Replacing the traditional blendshape and FLAME-based geometric control with a dense, per-pixel 3D position map representation, our method captures fine-grained facial details and subtle expression dynamics with significantly higher fidelity.

3. METHOD

Our objective is to decode continuous facial expressions from EEG signals. To achieve this, we first design a multi-modal data capture system (Section 3.1) and perform synchronized EEG-video data acquisition (Section 3.2) followed by signal and geometry preprocessing (Section 3.3).

Using the processed data, we develop an EEG encoder framework based on a convolutional transformer architecture [40], coupled with a decoder [33] that learns to map brain signals to facial geometry in the format of positional map (Section 3.4). Finally, the reconstructed EEG-driven meshes are rendered photorealistically using a variant of GaussianAvatars pipeline [31], enabling realistic and view-consistent avatar synthesis. Our overall framework is illustrated in Figure 2.

3.1. Data Capture Setup

Facial Performance Capturing. We record a participant’s responses to stimulus videos from multiple view points under a constant lighting condition. Sixteen cinema-grade global-shutter cameras (up to 8K resolution, 120 fps) are evenly distributed around the subject at 15° intervals, providing dense view coverage for photogrammetric reconstruction. A display positioned in front of the participant presents emotionally evocative video stimuli to elicit natural expressions. An illustration of our capture setup is shown in the supplementary materials. All cameras are synchronized using genlock and timecode generators to ensure precise temporal alignment across all views for high-fidelity performance reconstruction.

EEG Capturing Device. We use the Cyton-Daisy biosensing kit by OpenBCI for EEG data acquisition due to its portability and reliable signal quality. The device records 16-channel EEG signals at a sampling rate of 125Hz. Electrodes are positioned according to the international 10–20 system, as illustrated in the supplementary materials, providing evenly distributed coverage across the scalp. Although the number of channels is fewer than that of clinical-grade EEG systems, this configuration offers sufficient spatial resolution to capture representative neural activity across major cortical regions [1, 12], making it well-suited for our expression decoding task. Conductive gel is applied to each electrode to maintain impedance below 500k Ω , ensuring stable and high-quality signal acquisition.

Synchronization. Synchronization between the camera array and the EEG headset is achieved through a linear signal generated by an Arduino Teensy board, ensuring frame-accurate temporal alignment between EEG measurements and corresponding facial expressions. This setup yields a dual-modality dataset with precisely synchronized EEG and multi-view facial recordings, enabling reliable cross-modal learning.

3.2. Experiments Design and Data Acquisition

Stimulus Videos. The stimulus videos are manually selected from the Open Library for Affective Videos (OpenLAV) [11] and emotion eliciting clips curated by

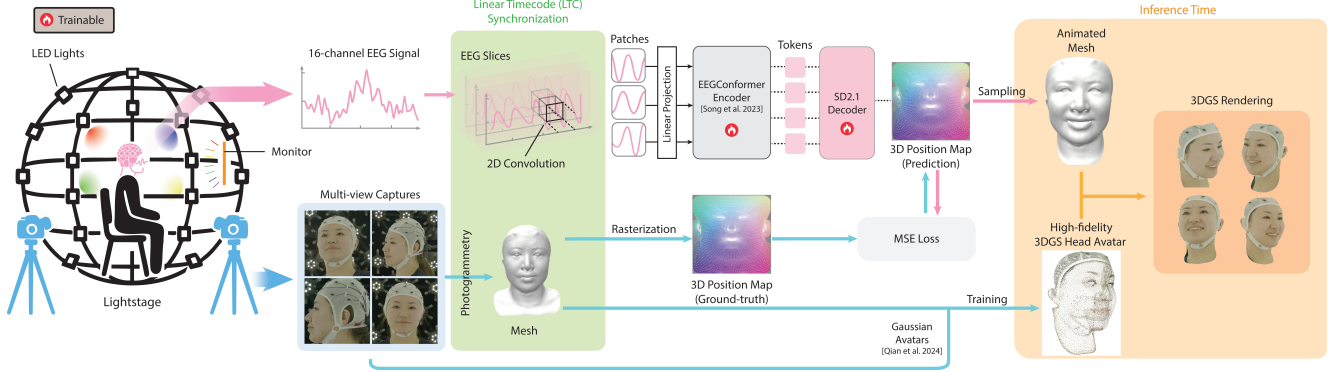


Figure 2. **Overview of Our Mind-to-Face Pipeline.** Our system decodes raw EEG signals into dense 3D position maps that are rendered into photorealistic avatars. Data are collected using a custom multi-view capture rig composed of synchronized high-speed RGB cameras and a 16-channel EEG headset, with all modalities temporally aligned via Linear Timecode for frame-accurate correspondence between EEG and facial expressions. Multi-view videos are reconstructed into ground-truth 3D facial meshes through photogrammetry. During training, EEG slices are encoded using a CNN-Transformer encoder (EEG-Conformer [40]) and decoded into 3D position maps using a Stable Diffusion 2.1 image decoder [33], supervised with MSE loss against photogrammetric position maps. At inference, the predicted position maps are resampled into meshes and rendered using a modified GaussianAvatars pipeline [31] for high-fidelity avatar synthesis.

Coan and Allen [4]. The selected clips are grouped into five emotion specific categories—neutral, disgust, funny, angry, and sad—each constituting a single trial in subsequent experiments. In addition, a separate video containing mixed emotional content is compiled from the EMOSTIM dataset [38] and used as a leave-one-trial-out testing sequence.

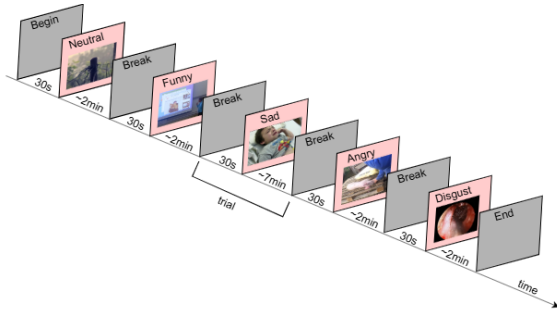


Figure 3. **Trial Design.** The experiment consists of five emotion-specific trials, each separated by a 30-second rest period. Within each trial, participants view a sequence of video clips conveying a single, consistent emotion corresponding to that trial’s theme.

Experiment Procedure. The subject is seated at the center of the Light Stage while wearing the EEG headset. The stage is uniformly illuminated under a high depth-of-field lighting configuration to minimize motion blur during performance capture. To ensure precise temporal alignment, stimulus playback, EEG recording, and multi-view video capture are initiated simultaneously. At the beginning of each trial, a prompt appears on the display indicating the target emotion category, preparing the subject’s mental state for the upcoming stimuli. The correspond-

ing stimulus videos are then presented, followed by a 30-second rest period between trials to prevent emotional carryover effects. Each subject completes five stimulus trials, as illustrated in Fig. 3, resulting in approximately 25 minutes of total recording time. The setup yields a synchronized dual-modality dataset comprising high-resolution multi-view videos and EEG signals. In total, around 30 minutes video data per-subject is captured in compressed RAW format from 16 synchronized cameras, producing roughly 7TB of data per subject. Despite the dataset’s large size and preprocessing demands, all recordings were successfully processed and prepared for decoding.

3.3. Preprocessing

EEG Preprocessing. For each trial, the raw EEG data is represented as a time-varying signal with C channels sampled at each time step. A 6th-order Butterworth band-pass filter with a passband of 4-40Hz is applied to suppress high-frequency noise and remove low-frequency drift and DC components introduced by the recording hardware. Per-channel z-score standardization is then performed using statistics computed from the training set, with the corresponding mean and variance applied to the test set for normalization consistency. The filtered and normalized EEG signals are subsequently segmented into overlapping temporal windows, each denoted as $E^{(t)} \in \mathbb{R}^{W \times C}$, where $W = 375$ is the window size, and $C = 16$. Each EEG window $E^{(t)}$ is temporally aligned with a corresponding ground-truth 3D position map $P^{(t)}$ reconstructed via multi-view photogrammetry.

Face Geometry Reconstruction. To enable supervised learning for decoding facial expressions, we reconstruct a 3D facial mesh $M^{(t)}$ for each video frame $I^{(t)}$ captured during the trial sessions. We track the subject’s performance by first solving for the facial identity of a neutral expression frame using the 3D Morphable Model (3DMM) from ICT-FaceModel [18], and then fitting the identity template mesh to the multi-view photogrammetry observations while maintaining consistent topology by Laplacian deformation. Optical flow-based refinement is also employed for temporal stability.

We apply a rigid Procrustes alignment using the Kabsch algorithm [13] to eliminate the head poses and align each reconstructed mesh to a canonical coordinate frame shared across all timesteps (see details in supplementary materials) to ensure that the decoder focuses on predicting non-rigid, expression-related deformations. For each aligned mesh $M^{(t)}$, we then generate a corresponding 3D position map $P^{(t)} \in \mathbb{R}^{256 \times 256 \times 3}$, where each pixel encodes the (x, y, z) coordinates of the facial surface in UV space. This representation preserves geometric continuity while enabling dense supervision for EEG decoding. Each position map is temporally aligned with its corresponding EEG window described in Sec. 3.3, forming paired samples $(E^{(t)}, P^{(t)})$ for training the EEG-to-face decoder in Sec. 3.4.

Neural Avatar Preprocessing. We convert the predicted 3D position maps $\hat{P}^{(t)}$ into meshes by sampling vertex coordinates $\hat{\mathbf{v}}^{(t)} \in \mathbb{R}^{V \times 3}$ to form meshes $\hat{M}^{(t)}$ according to the template UV layout. While the shared topology provides spatial consistency, the temporal smoothness of the reconstructed sequence primarily came from the overlapping EEG windows used during decoding, which yields gradually varying position maps over time. To prepare training data for GaussianAvatars, each mesh $M^{(t)}$ is projected onto the corresponding multi-view images to generate binary foreground masks, which are used to extract white-background facial crops $\{I_c^{(t)}\}$. The synchronized meshes $\{\mathbf{v}^{(t)}, \mathbf{f}\}$ and masked images $\{I_c^{(t)}\}$ are then used to train our modified GaussianAvatars model (see Sec. 3.5).

3.4. Decoding 3D Position Maps from EEG

To map EEG signals to dense 3D position maps, we first encode the preprocessed signals using a hybrid Convolution–Transformer architecture inspired by EEG-Conformer [40]. Each EEG slice $E^{(t)} \in \mathbb{R}^{W \times C}$ is reshaped into a single-channel tensor of size $1 \times C \times W$, which can be interpreted as a spatiotemporal image capturing both temporal dynamics and inter-channel structure. Following prior work [32, 35], we apply two sequential convolutional layers: the first along the temporal axis to model short-range temporal patterns, and the second across channels to capture spatial correlations between electrodes. The resulting

features pass through batch normalization, an ELU activation, and an average-pooling layer that reduces temporal redundancy and promotes more stable, emotion-relevant representations.

The resulting feature sequence is passed through a transformer encoder that models long-range temporal dependencies within the EEG window and outputs a compact latent embedding $\mathbf{z}^{(t)}$. Since a 3D position map is an image-like representation (similar to a depth map), an image decoder is a natural choice for reconstruction. We adapt the Stable Diffusion 2.1 [33] decoder (initialized from a pretrained checkpoint and fully finetuned) to generate the dense 3D position map $\hat{P}^{(t)}$, effectively bridging the spatiotemporal EEG domain with the spatial structure of the human face. A binary mask m restricts supervision to the inner-face region, encouraging the decoder to focus on expressive geometry. To further enhance surface smoothness and continuity, we include a self-supervised Laplacian regularization term (details in Supplementary Materials). The overall position map loss is defined as:

$$\mathcal{L}_{\text{pm}} = \lambda_{\text{rec}} \mathcal{L}_{\text{rec}} + \lambda_{\text{smooth}} \mathcal{L}_{\text{smooth}},$$

where \mathcal{L}_{rec} denotes the per-pixel mean squared error (MSE), and $\mathcal{L}_{\text{smooth}}$ represents the Laplacian smoothing loss applied to \hat{P} within the masked region.

3.5. Avatar Rendering with 3D Gaussian Splatting

We adopt 3DGS for neural head rendering, replacing traditional texture-based methods with a view-dependent representation that captures realistic lighting via spherical harmonics. In this framework, a scene is modeled as a set of ellipsoidal Gaussian splats parameterized by a covariance matrix Σ and center μ :

$$G(\mathbf{x}) = \exp\left(-\frac{1}{2}(\mathbf{x} - \mu)^T \Sigma^{-1}(\mathbf{x} - \mu)\right),$$

where Σ is defined by rotation $\mathbf{r} \in \mathbb{R}^{3 \times 3}$, scale $\mathbf{s} \in \mathbb{R}^3$, and position $\mu \in \mathbb{R}^3$. Each Gaussian’s color \mathbf{c} is modeled using 3rd-order spherical harmonics, and the final color is rendered by alpha compositing overlapping splats:

$$\mathbf{C} = \sum_{i=1} \mathbf{c}_i \alpha_i \prod_{j < i} (1 - \alpha_j')$$

At initialization, each triangular face of the mesh is assigned one Gaussian with local parameters $(\mathbf{r}, \mu, \mathbf{s})$, transformed into global coordinates during rendering as:

$$\mathbf{r}' = \mathbf{R}\mathbf{r}, \quad \mu' = k\mathbf{R}\mu + \mathbf{T}, \quad \mathbf{s}' = k\mathbf{s}, \quad (1)$$

where \mathbf{R} , \mathbf{T} , and k denote the face’s rotation, translation, and scale, respectively. This provides a geometry-aware initialization for stable reconstruction (see Fig. 4).

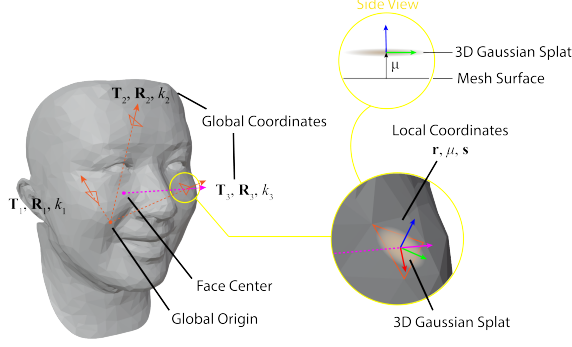


Figure 4. **Illustration of the Gaussian Binding Strategy.** Each ellipsoidal Gaussian splat is defined by its local rotation \mathbf{r} , position μ , and scale \mathbf{s} relative to the face center with global transform \mathbf{T} and \mathbf{R} . During animation, \mathbf{T} and \mathbf{R} are updated over time according to the predicted facial geometry, while \mathbf{r} , μ , and \mathbf{s} remain fixed as learnable parameters. The mesh is decimated for clarity in visualization.

At the training phase, we do not compute the face geometry from the tracked FLAME parameters as in [31]. Instead, we obtain directly the topology-consistent and facial geometry from our face tracking (see details in Sec. 3.3), since it offers greater flexibility and thus fits closer to the actual vibrant facial expressions. Our face tracking pipeline also improves upon the baseline in our scenario with occlusion and extreme expressions, demonstrated in Sec. 6.1. For each iteration, we sample a triplet of (mesh M , camera p , image I) uniformly at random, and render the Gaussian splats, each with the rigid transformation defined in Eq. 1 based on M . The properties are optimized with loss

$$\mathcal{L} = (1 - \lambda)\mathcal{L}_1 + \lambda\mathcal{L}_{\text{D-SSIM}} + \lambda_{\text{pos}}\mathcal{L}_{\text{pos}} + \lambda_{\text{scale}}\mathcal{L}_{\text{scale}}, \quad (2)$$

where \mathcal{L}_1 and $\mathcal{L}_{\text{D-SSIM}}$ compare the difference in the rendered images, $\mathcal{L}_{\text{pos}} = \|\max(\mu, \epsilon_{\text{pos}})\|_2$ regularizes the spatial shift from the face center that the splat is bound to, and $\mathcal{L}_{\text{scale}} = \|\max(\mathbf{s}, \epsilon_{\text{scale}})\|_2$ regularizes scales of the Gaussians. During rendering, we move and render the optimized splats by the mesh deformed according to the position maps (see Sec. 3.4). For 3DGS training, we use the same hyperparameters as documented in [31].

4. IMPLEMENTATION DETAILS

CNN-Transformer Encoder. Each EEG input window is represented as a tensor of shape $(B, 1, 16, 375)$, where 16 is the number of electrode channels and 375 is the temporal samples. The encoder begins with a temporal convolution $\text{Conv2d}(1, 40, (1, 25), (1, 1))$ that extracts short-range temporal patterns, followed by a spatial convolution $\text{Conv2d}(40, 40, (16, 1), (1, 1))$ spanning all channels to model spatial correlations between electrodes. The output is processed by $\text{BatchNorm2d}(40)$, an ELU nonlinearity, and an average pooling layer $\text{AvgPool2d}((1, 75), (1, 15))$

that reduces the temporal resolution while preserving essential dynamics. After pooling, the temporal dimension reduces from 375 to approximately 19 feature patches. A 1×1 convolution then projects the feature maps to an embedding dimension of $E = 40$, forming a sequence of tokens $\mathbf{z}_0^{(t)} \in \mathbb{R}^{B \times N \times E}$ with $N=19$.

The token sequence $\mathbf{z}_0^{(t)}$ is then processed by a stack of six transformer encoder layers. Each layer applies pre-normalization with *LayerNorm*, multi-head self-attention with 10 heads, and a feed-forward block that expands the embedding dimension by a factor of 4, with GELU activation and dropout ($p=0.5$). Residual connections are employed in both attention and feed-forward sublayers to stabilize optimization. The final output $\mathbf{z}^{(t)}$ encodes temporally integrated EEG features for time window t that are passed to the 3D position map decoder.

Image Decoder. To reconstruct dense 3D position maps from EEG-derived latent embeddings $\mathbf{z}^{(t)}$, we adapt the pre-trained *Stable Diffusion 2.1* variational autoencoder (VAE) as an image decoder. The decoder receives a flattened $\mathbf{z}^{(t)}$ of size $B \times d_{\text{in}}$, which is projected through a sequence of fully connected layers into a latent feature map of dimension $B \times 4 \times 8 \times 8$, matching the latent space of the Stable Diffusion VAE. The latent tensor is then decoded through the VAE into a coarse 3-channel output, followed by 2 transposed convolution layers to produce a dense 3D position map $\hat{P} \in \mathbb{R}^{256 \times 256 \times 3}$, where each pixel encodes the (x, y, z) coordinates of the reconstructed facial surface. The VAE parameters are initialized from the Stable Diffusion checkpoint but remain trainable to adapt the generative prior to the EEG feature domain. The predicted face mesh is then sampled from the 3D position map, which drives the trained Gaussian Splats attached to the faces to render the facial image.

5. EXPERIMENTS

Since there is no direct baseline to compare against, to the best of our knowledge, we report only our own quantitative and qualitative results to assess system performance. We evaluate reconstruction accuracy using nMAE/nRMSE against ground-truth position maps and present cross-subject visual results under different emotional stimuli. Together, these results demonstrate that our framework reliably maps EEG to expressive facial geometry and provide the first benchmark for future neural-to-avatar research to build upon.

5.1. Quantitative Evaluations

Each emotion trial consists of several stimulus videos presented sequentially to the subject, during which synchronized EEG and multi-view facial recordings are captured. For evaluation, we select all responses corresponding to the

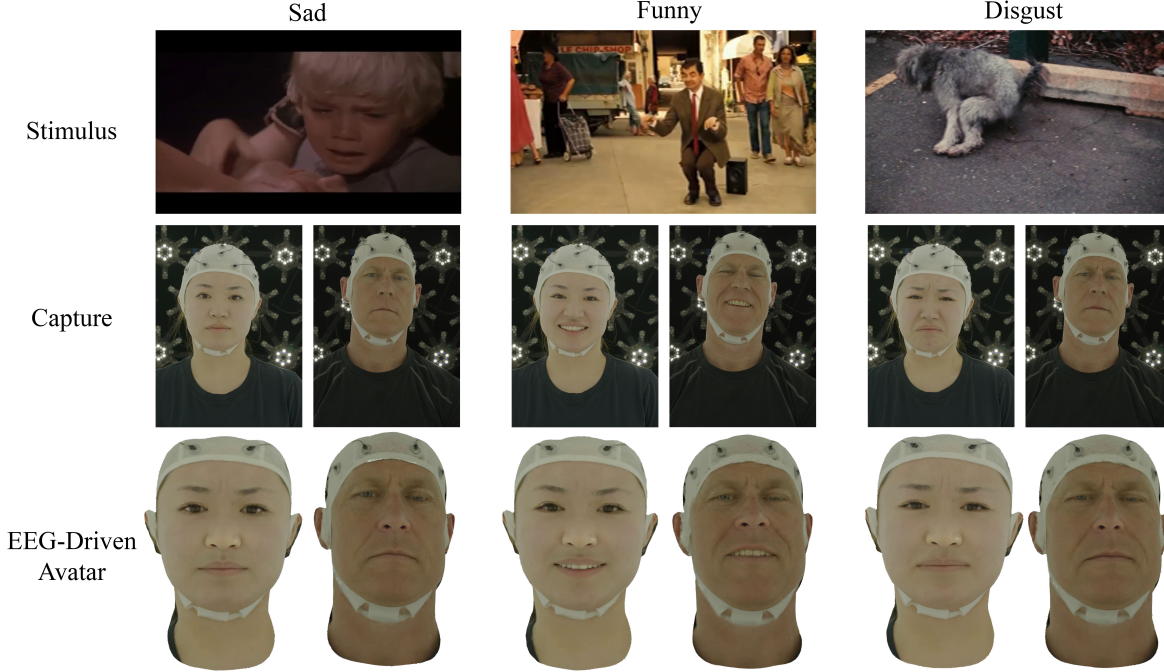


Figure 5. **Qualitative results of EEG-driven facial expression synthesis from testing set.** For three stimulus categories (Sad, Funny, Disgust), we show the emotion-eliciting video frames (top), the captured facial expressions from two subjects (middle), and the corresponding expressions produced by our EEG-driven avatar (bottom). The reconstructed avatars reflect subject-specific emotional responses and capture both neutral and strongly expressive frames. More qualitative results and video demos can be found in Supplementary Materials.

final stimulus video of each trial as the testing set, while the responses from the remaining videos are used for training, resulting in approximately 85% training and 15% testing data. This strategy ensures that EEG segments in the test set are temporally disjoint from those in the training set, providing a fair assessment of the model’s ability to generalize across time within the same emotional category.

Although our preprocessing pipeline adheres to standard signal processing practices designed to minimize statistical leakage, subtle forms of data dependency across time or stimuli may still arise. To further ensure the robustness of evaluation, we include a standalone *EMOSTIM* (see Sec. 3.2) sequence recorded under a distinct set of mixed-emotion stimulus videos, which is excluded entirely from training and used solely to assess cross-trial generalization. For each EEG window, the network predicts a dense 3D position map $\hat{P}^{(t)} \in \mathbb{R}^{256 \times 256 \times 3}$, evaluated against the corresponding ground-truth map $P^{(t)}$ reconstructed from multi-view photogrammetry. Performance is reported in Tab. 1 using per-pixel normalized Mean Absolute Error¹ (nMAE) and normalized Root Mean Squared Error (nRMSE) within the inner-face mask.

¹Normalized MAE expresses the average absolute error as a fraction of the ground-truth value range. For example, nMAE=0.001 means predictions deviate by 0.1% of the ground-truth’s amplitude span-roughly 0.1mm

Subject	Lillian		Rob	
Trial	nMAE↓	nRMSE↓	nMAE↓	nRMSE↓
Funny	0.00370	0.00559	0.00476	0.00641
Disgust	0.00421	0.00585	0.00264	0.00393
Sad	0.00169	0.00285	0.00111	0.00218
Angry	0.00244	0.00372	0.00222	0.00332
Neutral	0.00207	0.00326	0.00143	0.00253
EMOSTIM	0.00254	0.00386	0.00523	0.00721

Table 1. **Quantitative results of position map prediction.** Testing-set normalized Mean Absolute Error (nMAE) and normalized Root Mean Squared Error (nRMSE) are reported for both subjects as a baseline for future work. The EMOSTIM sequence serves as a leave-one-out trial for cross-trial generalization.

5.2. Qualitative Results

We show qualitative results (see Fig. 5) for two subjects across three stimulus types (sad, funny, disgust). The EEG-driven avatars reproduce the main facial changes for each case (e.g., frown for sadness, smiles for funny clips, brow/nose tightening for disgust) while keeping each person’s identity. Despite differences in how each person re-

if the underlying 3D offsets vary over 10cm.

sponds to the same stimulus, the decoded position maps adapt to subject-specific dynamics such as the smile intensity, indicating effective personalization rather than stimulus memorization.

For GS-based avatar rendering, we further refine the mouth interior using a pretrained GFPGAN [48] model, following the post-processing strategies adopted in recent neural avatar works [22, 47]. Multi-view rendering and video results are provided in the Supplementary Material.

6. ABLATION STUDIES

6.1. Comparison with GaussianAvatars

The GaussianAvatars pipeline is optimal in the common scenario where the expressions are mild and the majority of the face is clear. However, in our setting, to capture synchronized image and EEG data, it is necessary for the subjects to wear a headcap with sensors, which may confuse common facial landmark decoders, such as the VHAP library [30] used in their pipeline; the extreme expressions, triggered by the emotion-eliciting videos we use, are often beyond the expressivity of FLAME parameters [20]. Therefore, as Fig. 6 shows, we conclude that the standard GaussianAvatar pipeline does not generalize to our data capture setup, and it may predict inaccurate expressions (b) or even fail catastrophically (c), whereas our method maintains robustness in the complex capture settings.

6.2. Why Position Maps Instead of Blendshapes?

A natural baseline for EEG-driven facial animation is to regress a low-dimensional blendshape vector (typically 52 coefficients). However, blendshapes encode only a fixed set of predefined muscle-driven motions and cannot capture high-frequency, subject-specific geometry such as wrinkles or creases. In contrast, a 3D position map provides a dense $256 \times 256 \times 3$ representation of surface geometry, with over 2×10^5 degrees of freedom, offering far greater capacity to model fine-grained deformations.

Figure 7 illustrates this difference. When the subject raises her brows, the blendshape reconstruction yields an overly smooth forehead, missing the subtle yet emotionally meaningful patterns. The position map-based prediction, by comparison, preserves these local geometric variations and more closely matches the ground-truth expression.

7. CONCLUSIONS AND FUTURE WORK

Conclusion. We introduce *Mind-to-Face*, the first framework to map non-invasive EEG signals directly to photorealistic 3D facial expressions. By decoding EEG into dense 3D position maps and rendering them with 3D Gaussian Splatting, we show that high-fidelity, subject-specific facial animation can be driven entirely from neural activity. A

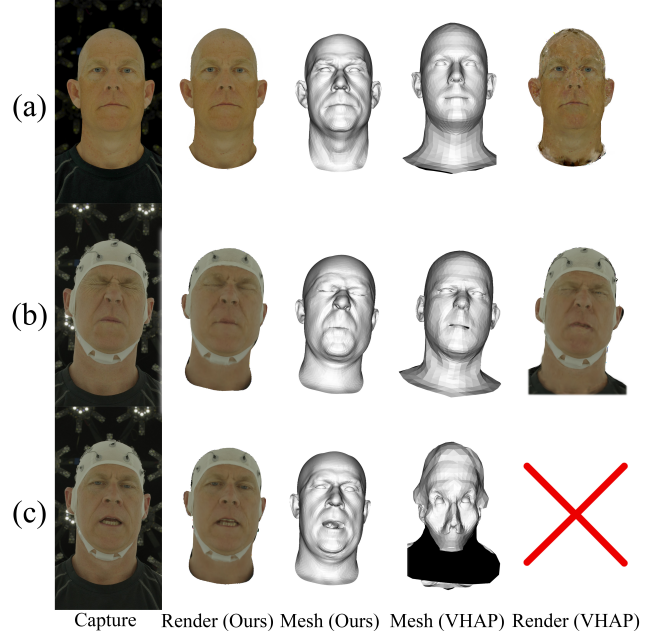


Figure 6. **We demonstrate that the face tracking pipeline of GaussianAvatars does not suit our scenario.** In (a), we show that in an occlusion-free scenario, the avatar rendered by our pipeline is similar to that of GaussianAvatars. However, in our complex capture setup with extreme expressions and headcap-induced occlusion, errors in landmark detection of the GaussianAvatars pipeline can lead to incorrect expression tracking (b) or even completely broken geometry (c). The red cross indicates that the model fails to produce a faithful render due to collapsed geometry.

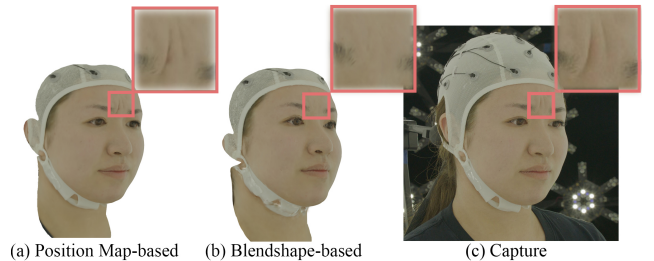


Figure 7. **Blendshape parameters cannot reflect subtle details.** We compare EEG-driven facial reconstruction using our position-map decoder (a) with a standard 52-dimensional blendshape regressor (b), alongside the ground-truth capture (c). The highlighted forehead region shows that blendshape-based reconstruction fails to reproduce fine-grained expressive details, such as wrinkles, due to its limited degrees of freedom. In contrast, the dense position map preserves subtle geometric deformations, resulting in nuanced expression reconstruction.

synchronized dual-modality capture setup provides the precise EEG–video alignment needed for supervised learning. Together, these components establish a unified pipeline for neural-driven avatars, enabling new directions in affective computing, telepresence, and brain–computer interfaces.

Future Work. We plan to extend this framework along two directions. First, we will collect a larger multimodal dataset with more subjects and a broader set of emotional and cognitive stimuli. This will increase statistical robustness, enable cross-subject generalization, and support deeper analysis of individual variability in neural-driven facial expressions. Second, we aim to incorporate stimulus content as an additional conditioning signal during decoding. Joint modeling of EEG responses and stimulus context may help disentangle perceptual and affective components, leading to more precise and context-aware facial synthesis.

References

- [1] Shideh Kabiri Ameri, Myungsoo Kim, Irene Agnes Kuang, Withanage K Perera, Mohammed Alshiekh, Hyoyoung Jeong, Ufuk Topcu, Deji Akinwande, and Nanshu Lu. Imperceptible electrooculography graphene sensor system for human–robot interface. *npj 2D Materials and Applications*, 2(1):19, 2018. [3](#)
- [2] Volker Blanz and Thomas Vetter. A morphable model for the synthesis of 3d faces. In *Proceedings of the 26th annual conference on Computer graphics and interactive techniques*, pages 187–194, 1999. [3](#)
- [3] Caroline Chan, Shiry Ginosar, Tinghui Zhou, and Alexei A Efros. Everybody Dance Now. pages 5933–5942, 2019. [3](#)
- [4] James A Coan and John JB Allen. *Handbook of emotion elicitation and assessment*. Oxford university press, 2007. [4](#)
- [5] Ruo-Nan Duan, Jia-Yi Zhu, and Bao-Liang Lu. Differential entropy feature for eeg-based emotion classification. pages 81–84, 2013. [2](#)
- [6] Paul Ekman. An argument for basic emotions. *Cognition and Emotion*, 6(3-4):169–200, 1992. [2](#)
- [7] Jérémy Frey. Comparison of an open-hardware electroencephalography amplifier with medical grade device in brain-computer interface applications. *arXiv preprint arXiv:1606.02438*, 2016. [1](#)
- [8] Guy Gafni, Justus Thies, Michael Zollhöfer, and Matthias Nießner. Dynamic neural radiance fields for monocular 4d facial avatar reconstruction. In *Proceedings of the IEEE/CVF Conference on Computer Vision and Pattern Recognition (CVPR)*, pages 8649–8658, 2021. [3](#)
- [9] Philip-William Grassal, Malte Prinzler, Titus Leistner, Carsten Rother, Matthias Nießner, and Justus Thies. Neural head avatars from monocular rgb videos, 2022. [3](#)
- [10] Liangxiao Hu, Hongwen Zhang, Yuxiang Zhang, Boyao Zhou, Boning Liu, Shengping Zhang, and Liqiang Nie. Gaussianavatar: Towards realistic human avatar modeling from a single video via animatable 3d gaussians. In *IEEE/CVF Conference on Computer Vision and Pattern Recognition (CVPR)*, 2024. [3](#)
- [11] Laura Israel, Philipp Paukner, Lena Schiestel, Klaus Diepold, and Felix Schönbrodt. Open library for affective videos (OpenLAV), 2021. [3](#)
- [12] Linxing Jiang, Andrea Stocco, Darby M Losey, Justin A Abernethy, Chantel S Prat, and Rajesh P N Rao. BrainNet: A Multi-Person Brain-to-Brain Interface for Direct Collaboration Between Brains. *Scientific Reports*, 9(1):6115, 2019. [3](#)
- [13] W. Kabsch. A solution for the best rotation to relate two sets of vectors. *Acta Crystallographica Section A*, 32(5):922–923, 1976. [5](#)
- [14] Bernhard Kerbl, Georgios Kopanas, Thomas Leimkühler, and George Drettakis. 3d gaussian splatting for real-time radiance field rendering, 2023. [1](#), [2](#), [3](#)
- [15] Hyeonwoo Kim, Pablo Garrido, Ayush Tewari, Weipeng Xu, Justus Thies, Matthias Nießner, Patrick Pérez, Christian Richardt, Michael Zollöfer, and Christian Theobalt. Deep video portraits. *ACM Transactions on Graphics (TOG)*, 37(4):163, 2018. [3](#)
- [16] Vernon J Lawhern, Amelia J Solon, Nicholas R Waytowich, Stephen M Gordon, Chou P Hung, and Brent J Lance. Eeg-net: a compact convolutional neural network for eeg-based brain–computer interfaces. *Journal of Neural Engineering*, 15(5):056013, 2018. [2](#)
- [17] Hao Li, Laura Trutoiu, Kyle Olszewski, Lingyu Wei, Tristan Trutna, Pei-Lun Hsieh, Aaron Nicholls, and Chongyang Ma. Facial-performance-sensing head-mounted display. 2015. [2](#)
- [18] Ruilong Li, Karl Bladin, Yajie Zhao, Chinmay Chinara, Owen Ingraham, Pengda Xiang, Xinglei Ren, Pratusha Prasad, Bipin Kishore, Jun Xing, et al. Learning formation of physically-based face attributes, 2020. [5](#)
- [19] Rui Li, Di Liu, Zhijun Li, Jinli Liu, Jinciao Zhou, Weiping Liu, Bo Liu, Weiping Fu, and Ahmad Bala Alhassan. A novel EEG decoding method for a facial-expression-based BCI system using the combined convolutional neural network and genetic algorithm. *Frontiers in Neuroscience*, 16: 988535, 2022. [2](#)
- [20] Tianye Li, Timo Bolkart, Michael J. Black, Hao Li, and Javier Romero. Learning a model of facial shape and expression from 4D scans. *ACM Transactions on Graphics, (Proc. SIGGRAPH Asia)*, 36(6):194:1–194:17, 2017. [2](#), [3](#), [8](#)
- [21] Xiaotian Li, Xiang Zhang, Huiyuan Yang, Wenna Duan, Weiying Dai, and Lijun Yin. An eeg-based multi-modal emotion database with both posed and authentic facial actions for emotion analysis. In *2020 15th IEEE International Conference on Automatic Face and Gesture Recognition (FG 2020)*, page 336–343. IEEE, 2020. [2](#)
- [22] Xueting Li, Shalini De Mello, Sifei Liu, Koki Nagano, Umar Iqbal, and Jan Kautz. Generalizable one-shot 3d neural head avatar. *Advances in Neural Information Processing Systems*, 36:47239–47250, 2023. [8](#), [3](#)
- [23] Shichen Liu, Yunxuan Cai, Haiwei Chen, Yichao Zhou, and Yajie Zhao. Rapid face asset acquisition with recurrent feature alignment. *ACM Transactions on Graphics (TOG)*, 41(6):1–17, 2022. [2](#)
- [24] Yisi Liu, Olga Sourina, and Minh Khoa Nguyen. Real-time eeg-based human emotion recognition and visualization. In *Proceedings of the 2010 International Conference on Cyberworlds*, page 262–269, USA, 2010. IEEE Computer Society. [2](#)
- [25] Ben Mildenhall, Pratul P Srinivasan, Matthew Tancik, Jonathan T Barron, Ravi Ramamoorthi, and Ren Ng. Nerf: Representing scenes as neural radiance fields for view synthesis, 2021. [3](#)
- [26] Gyeongsik Moon, Takaaki Shiratori, and Shunsuke Saito. Expressive whole-body 3d gaussian avatar, 2024. [3](#)
- [27] Maryam Nadeem, Raza Imam, Rouqaiyah Al-Refai, Meriem Chkir, Mohamad Hoda, and Abdulmotaleb El Saddik. EVOKE: Emotion Enabled Virtual Avatar Mapping Using Optimized Knowledge Distillation. pages 1–6, 2024. [2](#)
- [28] Jerrin Thomas Panachakel, Ranjana H, Sana Parveen K, Sidharth Sidharth, and Ashish Abraham Samuel. Csp- lstm based emotion recognition from eeg signals. In *2023 IEEE International Conference on Metrology for eXtended Reality, Artificial Intelligence and Neural Engineering (MetroX-RAINE)*, pages 289–294, 2023. [2](#)

- [29] Filip Postepski, Grzegorz M Wojcik, Krzysztof Wrobel, Andrzej Kawiak, Katarzyna Zemla, and Grzegorz Sedek. Recurrent and convolutional neural networks in classification of eeg signal for guided imagery and mental workload detection, 2025. [2](#)
- [30] Shenhan Qian. Vhap: Versatile head alignment with adaptive appearance priors, 2024. [8](#)
- [31] Shenhan Qian, Tobias Kirschstein, Liam Schoneveld, Davide Davoli, Simon Giebenhain, and Matthias Nießner. Gaussianavatars: Photorealistic head avatars with rigged 3d gaussians, 2024. [2](#), [3](#), [4](#), [6](#)
- [32] Mouad Riyad, Mohammed Khalil, and Abdellah Adib. Micegnet: A novel convolutional neural network for motor imagery classification. *Journal of Neuroscience Methods*, 353: 109037, 2021. [2](#), [5](#)
- [33] Robin Rombach, Andreas Blattmann, Dominik Lorenz, Patrick Esser, and Björn Ommer. High-resolution image synthesis with latent diffusion models, 2022. [3](#), [4](#), [5](#)
- [34] James A. Russell. A circumplex model of affect. *Journal of Personality and Social Psychology*, 39(6):1161–1178, 1980. [2](#)
- [35] Robin Tibor Schirrmeister, Jost Tobias Springenberg, Lukas Dominique Josef Fiederer, Martin Glasstetter, Katharina Eggensperger, Michael Tangermann, Frank Hutter, Wolfram Burgard, and Tonio Ball. Deep learning with convolutional neural networks for eeg decoding and visualization. *Human Brain Mapping*, 38(11):5391–5420, 2017. [5](#)
- [36] Mohammad Soleymani, Jeroen Lichtenauer, Thierry Pun, and Maja Pantic. A multimodal database for affect recognition and implicit tagging. *IEEE Transactions on Affective Computing*, 3(1):42–55, 2012. [2](#)
- [37] Teresa Sollfrank, Oona Kohnen, Peter Hilfiker, Lorena C. Kegel, Hennric Jokeit, Peter Brugger, Miriam L. Loertscher, Anton Rey, Dieter Mersch, Joerg Sternagel, Michel Weber, and Thomas Grunwald. The Effects of Dynamic and Static Emotional Facial Expressions of Humans and Their Avatars on the EEG: An ERP and ERD/ERS Study. *Frontiers in Neuroscience*, 15:651044, 2021. [2](#)
- [38] Rukshani Somarathna, Patrik Vuilleumier, and Gelareh Mohammadi. Emostim: A database of emotional film clips with discrete and componential assessment. *IEEE Trans. Affect. Comput.*, 15(3):1202–1212, 2024. [4](#)
- [39] Yonghao Song, Xueyu Jia, Lie Yang, and Longhan Xie. Transformer-based spatial-temporal feature learning for EEG decoding. *arXiv preprint arXiv:2106.11170*, 2021. [2](#)
- [40] Yonghao Song, Qingqing Zheng, Bingchuan Liu, and Xiaorong Gao. EEG conformer: Convolutional transformer for EEG decoding and visualization. *IEEE Transactions on Neural Systems and Rehabilitation Engineering*, 31:710–719, 2023. [2](#), [3](#), [4](#), [5](#)
- [41] Olga Sorkine, Daniel Cohen-Or, Yaron Lipman, Marc Alexa, Christian Rössl, and H-P Seidel. Laplacian surface editing. In *Proceedings of the 2004 Eurographics/ACM SIGGRAPH symposium on Geometry processing*, pages 175–184, 2004. [3](#)
- [42] Congzhong Sun and Chaozhou Mou. Survey on the research direction of EEG-based signal processing. *Frontiers in Neuroscience*, 17:1203059, 2023. [2](#)
- [43] Supasorn Suwajanakorn, Steven M. Seitz, and Ira Kemelmacher-Shlizerman. Synthesizing obama: learning lip sync from audio. *ACM Trans. Graph.*, 36(4), 2017. [3](#)
- [44] Jiapeng Tang, Davide Davoli, Tobias Kirschstein, Liam Schoneveld, and Matthias Niessner. Gaf: Gaussian avatar reconstruction from monocular videos via multi-view diffusion, 2025. [3](#)
- [45] Justus Thies, Michael Zollhofer, Marc Stamminger, Christian Theobalt, and Matthias Nießner. Face2Face: Real-time Face Capture and Reenactment of RGB Videos. pages 2387–2395, 2016. [3](#)
- [46] Justus Thies, Michael Zollhöfer, and Matthias Nießner. Deferred Neural Rendering: Image Synthesis using Neural Textures. *Acm Transactions on Graphics (TOG)*, 38(4):1–12, 2019. [3](#)
- [47] Phong Tran, Egor Zakharov, Long-Nhat Ho, Anh Tuan Tran, Liwen Hu, and Hao Li. Voodoo 3d: Volumetric portrait disentanglement for one-shot 3d head reenactment. In *Proceedings of the IEEE/CVF Conference on Computer Vision and Pattern Recognition*, pages 10336–10348, 2024. [8](#), [3](#)
- [48] Xintao Wang, Yu Li, Honglun Zhang, and Ying Shan. Towards real-world blind face restoration with generative facial prior. In *Proceedings of the IEEE/CVF conference on computer vision and pattern recognition*, pages 9168–9178, 2021. [8](#), [3](#)
- [49] Jonathan R. Wolpaw, José del R. Millán, and Nick F. Ramsey. Chapter 2 - brain-computer interfaces: Definitions and principles. In *Brain-Computer Interfaces*, pages 15–23. Elsevier, 2020. [2](#)
- [50] Yuelang Xu, Hongwen Zhang, Lizhen Wang, Xiaochen Zhao, Han Huang, Guojun Qi, and Yebin Liu. LatentAvatar: Learning Latent Expression Code for Expressive Neural Head Avatar. pages 1–10, 2023. [3](#)
- [51] Ye Yuan, Xueting Li, Yangyi Huang, Shalini De Mello, Koki Nagano, Jan Kautz, and Umar Iqbal. Gavatar: Animatable 3d gaussian avatars with implicit mesh learning. pages 896–905, 2024. [3](#)
- [52] Yuchan Zhang, Guanghui Yan, Wenwen Chang, Wenjie Huang, and Yueting Yuan. Eeg-based multi-frequency band functional connectivity analysis and the application of spatio-temporal features in emotion recognition. *Biomedical Signal Processing and Control*, 79:104157, 2023. [2](#)
- [53] Wei-Long Zheng and Bao-Liang Lu. Investigating critical frequency bands and channels for EEG-based emotion recognition with deep neural networks. *IEEE Transactions on Autonomous Mental Development*, 7(3):162–175, 2015. [2](#)
- [54] Wei-Long Zheng and Bao-Liang Lu. A multimodal approach to estimating vigilance using eeg and forehead eeg. *Journal of Neural Engineering*, 14(2):026017, 2017. [2](#)
- [55] Wei-Long Zheng, Wei Liu, Yifei Lu, Bao-Liang Lu, and Andrzej Cichocki. Emotionmeter: A multimodal framework for recognizing human emotions. *IEEE Transactions on Cybernetics*, 49(3):1110–1122, 2018. [2](#)
- [56] Yufeng Zheng, Victoria Fernández Abrevaya, Marcel C. Bühler, Xu Chen, Michael J. Black, and Otmar Hilliges. I M Avatar: Implicit morphable head avatars from videos. In *Computer Vision and Pattern Recognition (CVPR)*, 2022. [3](#)

- [57] Wojciech Zielonka, Timur Bagautdinov, Shunsuke Saito, Michael Zollhöfer, Justus Thies, and Javier Romero. Drivable 3d gaussian avatars, 2025. [3](#)

Mind-to-Face: Neural-Driven Photorealistic Avatar Synthesis via EEG Decoding

Supplementary Material

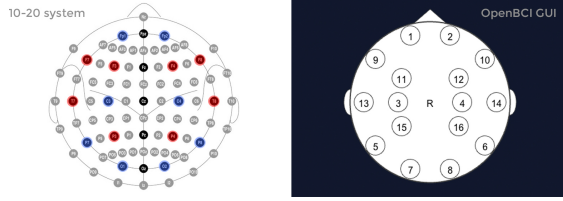


Figure 8. **EEG Channel Definition.** The channels recorded by the OpenBCI device [7] (shown on the right) correspond to the electrodes marked red or blue in the 10-20 system on the left.

A. More Qualitative Results

We provide additional qualitative results in Fig. 11, highlighting the multi-view consistency and 3D expressiveness of our EEG-driven avatar. Despite relying solely on neural signals, the model faithfully reproduces subjects’ reactions to the stimulus videos, generating realistic facial motion across multiple camera viewpoints. All examples shown are from the held-out test splits of each emotion trial.

We also include supplementary videos for both subjects that visualize the stimulus clips, their recorded reactions, and our predicted renderings for the standalone *EMOSTIM* trial.

B. EEG Cap Electrode Placement

The 10-20 system is a widely adopted international standard for electrode placement in electroencephalography (EEG), ensuring consistent and comprehensive coverage of the scalp for capturing neural signals. Electrodes are positioned based on anatomical landmarks at fixed percentages (10% and 20%) of the total distance across the head, which allows for standardized spatial distribution across key cortical regions. In our setup, we use 16 channels selected from this system, targeting a broad range of brain areas to balance spatial coverage with hardware simplicity. As shown in Fig. 8, the chosen electrodes span frontal (Fp1, Fp2, F7, F8, F3, F4), temporal (T7, T8), central (C3, C4), parietal (P3, P4), and occipital (O1, O2) regions, enabling the system to capture both cognitive and affective brain activity relevant to facial expression decoding. These 16 electrodes are mapped to the corresponding channel indices in the OpenBCI GUI, as visualized on the right in the figure.

C. Lightstage Setup

We perform volumetric capture in a light stage equipped with 16 high-speed, hardware-synchronized RGB cameras. For this work, we operate the stage under constant, flat illu-

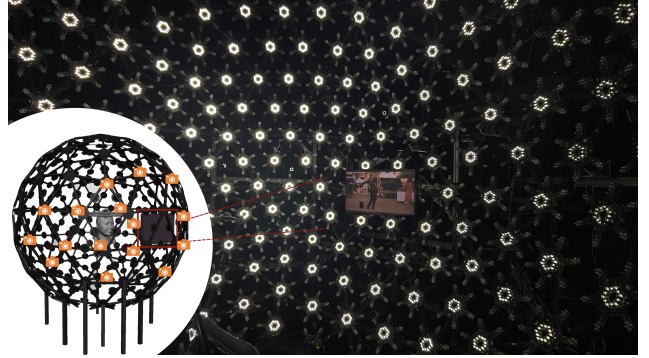


Figure 9. **Capture System.** We record each subject’s facial performance in a Light Stage with 16 synchronized cameras. This multi-view setup captures high-quality, temporally aligned imagery, enabling accurate photogrammetric reconstruction of high-fidelity facial meshes.

mination; however, the system supports fully programmable relighting for future works since each light source is individually controllable with known directions. A representative illustration of our setup is shown in Fig. 9.

During recording, the participant wearing the EEG head-cap and auxiliary is seated at the center of the stage and watches the stimulus videos described in Sec. 3.1. For each subject, we capture approximately 30 minutes of reaction footage. Although the cameras support 60 fps, we record at 30 fps with 8K resolution to balance expression coverage with storage and processing cost. A front-mounted monitor and speaker present the stimuli to the participant.

All modalities—the stimulus playback, EEG recordings, and multi-view camera streams—are temporally aligned using a time-code generator that provides a shared start signal. In total, the system captures synchronized EEG and facial expression data for two subjects, yielding 81,766 frames of high-resolution multi-view imagery.

D. Detailed EEG to Position Map Decoder Loss

Let $P \in \mathbb{R}^{H \times W \times 3}$ denote the ground-truth position map, \hat{P} the predicted position map, and $m \in \{0, 1\}^{H \times W}$ a binary mask selecting the inner-face region. The reconstruction loss is defined as:

$$\mathcal{L}_{\text{rec}} = \frac{1}{3HW} \|m \odot (\hat{P} - P)\|_2^2.$$

To promote spatial smoothness of \hat{P} within the masked region, we apply a discrete Laplacian operator $\mathcal{L}(\cdot)$ over each spatial channel to penalize rapid local variations:

$$\mathcal{L}_{\text{smooth}} = \frac{1}{3HW} \sum_{c=1}^3 \|m \odot \mathcal{L}(\hat{P}_{[:, :, c]})\|_2$$

The overall loss for position map decoding is then:

$$\mathcal{L} = \lambda_{\text{rec}} \mathcal{L}_{\text{rec}} + \lambda_{\text{smooth}} \mathcal{L}_{\text{smooth}}$$

Here, $\hat{P}_{[:, :, c]}$ refers to the c -th spatial channel of the predicted position map \hat{P} (i.e., the x , y , or z coordinate map).

This Laplacian regularizer acts as a surface smoothness constraint that reduces high-frequency noise while maintaining detailed local deformations consistent with expressive regions.

E. Rigid Procrustes Alignment via the Kabsch Algorithm

Given two meshes with identical topology, let

$$X = \{x_i\}_{i=1}^N, \quad Y = \{y_i\}_{i=1}^N, \quad x_i, y_i \in \mathbb{R}^3,$$

denote corresponding vertex sets. The goal is to estimate the optimal rotation $R \in \mathbb{R}^{3 \times 3}$ and translation $t \in \mathbb{R}^3$ that best align X to Y in the least-squares sense:

$$\min_{R, t} \sum_{i=1}^N \|y_i - (Rx_i + t)\|^2, \quad \text{s.t. } R^\top R = I, \det(R) = 1.$$

The alignment is computed using the classical Kabsch algorithm as shown in Algorithm 1.

Applying the transformation to all vertices yields the aligned mesh:

$$x'_i = Rx_i + t, \quad i = 1, \dots, N.$$

This procedure is applied independently to every mesh frame, aligning all sequences to a common canonical space while preserving vertex order and mesh topology.

Algorithm 1 Rigid Procrustes Alignment (Kabsch)

Require: Corresponding vertex sets $X, Y \in \mathbb{R}^{N \times 3}$

Ensure: Rotation matrix R and translation vector t

1: Compute centroids:

$$\mu_X = \frac{1}{N} \sum_i x_i, \quad \mu_Y = \frac{1}{N} \sum_i y_i$$

2: Center the point sets:

$$X_c = X - \mu_X, \quad Y_c = Y - \mu_Y$$

3: Form the covariance matrix:

$$H = X_c^\top Y_c$$

4: Compute SVD:

$$H = USV^\top$$

5: Compute rotation:

$$R = VU^\top$$

6: Ensure a proper rotation (no reflection):

$$\text{if } \det(R) < 0 : V_{:,3} \leftarrow -V_{:,3}, \quad R = VU^\top$$

7: Compute translation:

$$t = \mu_Y - R\mu_X$$

8: **return** R, t

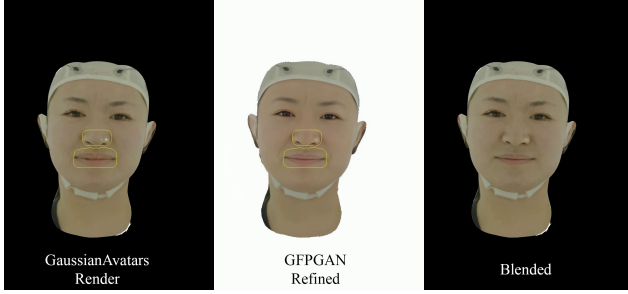


Figure 10. **Masked Blending.** Left to right: GaussianAvatars [31] rendering from EEG-predicted geometry; GFPGAN-refined frame; and the final blended result. Yellow boxes indicate the regions where refinement is selectively blended back into the original rendering.

F. GFPGAN & Masked Blending

Inspired by prior neural-avatar pipelines [22, 47], we apply a pretrained GFPGAN v1.3 model [48] to enhance the mouth region. We apply the public v1.3 model and input the 3DGS rendering for restoration. Since this refinement is applied in a per-frame manner, it may introduce minor temporal inconsistency. To mitigate this, we adopt a pyramid-blending strategy: artifact-prone regions are replaced with the refined outputs and smoothly blended back into the original renderings to maintain temporal and spatial coherence.

G. Template Fitting for Outer-Face Regions

Since outer-face regions are largely unaffected by expression changes, they are excluded from our position-map prediction model and instead filled using a generic template mesh. Starting from the sequence of position maps produced by our EEG decoder, each containing only the central facial area, we estimate subject-specific shape parameters using a linear 3D morphable-model (3DMM) fitting procedure, similar to [2]. The regression is performed only on vertices within the central region that have valid correspondences in the predicted position maps, yielding an initial shape aligned to the template topology.

To propagate these deformations to the remaining facial areas, we perform a non-rigid Laplacian deformation on the template mesh. Vertices within the central region serve as positional constraints, while a Laplacian regularizer enforces smooth deformation over the outer-face regions and non-facial components (e.g., eyeballs, mouth interior, accessory geometry). We adopt a variant of the Laplacian editing framework of [41] to solve this optimization, ensuring a geometrically coherent, full-face mesh suitable for downstream GaussianAvatar rendering.

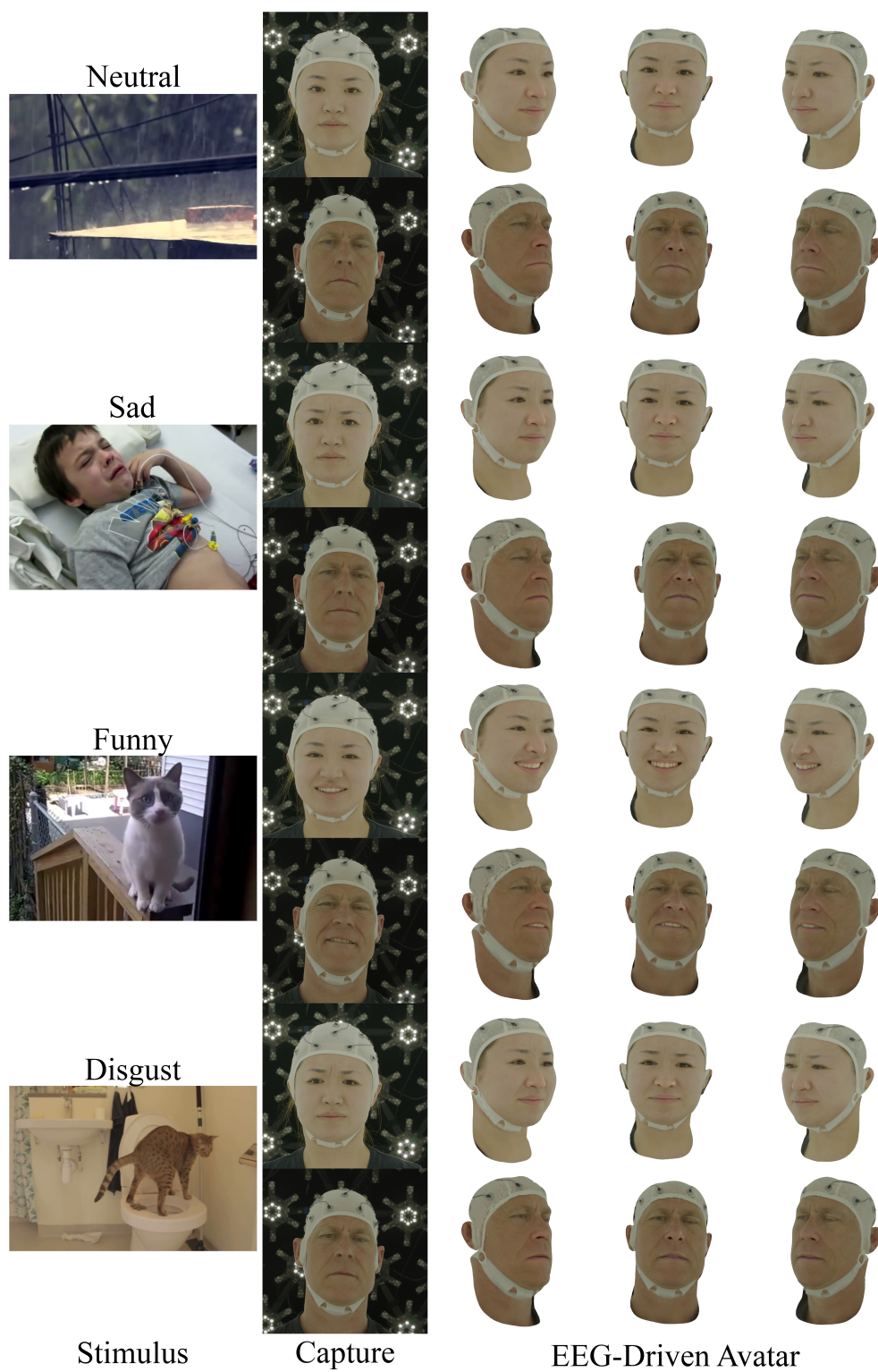


Figure 11. **Additional Qualitative Results and Multi-view Renders.** We show the reactions of both subjects (middle) to the stimulus frames (left). On the right are renders from multiple views of the predicted emotions by EEG signals.